

Dynamical correlations in multiorbital Hubbard models: Fluctuation-exchange approximations

V. Drchal, V. Janiš, and J. Kudrnovský

*Institute of Physics, AS CR, Na Slovance 2, CZ-182 21 Praha 8, Czech Republic**

V. S. Oudovenko, X. Dai and K. Haule, and G. Kotliar
*Center for Materials Theory, Department of Physics and Astronomy,
 Rutgers University, Piscataway, New Jersey 08854*

(Dated: February 7, 2020)

We study the two band degenerate Hubbard model using the Fluctuation Exchange approximation (FLEX) method and compare the results with Quantum Monte-Carlo (QMC) calculations. Both the self-consistent and the non-self-consistent versions of the FLEX scheme are investigated. We find that, contrary to the one band case, in the multiband case, good agreement with the Quantum Monte-Carlo results is obtained within the electron-electron T -matrix approximation using the full renormalization of the one-particle propagators. The crossover to strong coupling and the formation of satellites is more clearly visible in the non-self-consistent scheme. Finally we discuss the behavior of the FLEX for higher orbital degeneracy.

PACS numbers: 71.10.-w, 71.10.Fd, 71.27.+a

I. INTRODUCTION

Recent progress in the development and application of advanced experimental techniques made available a number of new materials and compounds with strongly correlated electrons that cannot be entirely described within the Density Functional Theory (DFT)^{1,2}. Some transition-metal alloys, cuprates, manganites, heavy-fermion Kondo and mixed-valence systems, as well as lanthanides and transuranium compounds behave in a way that can neither be explained nor understood within first-principles computational schemes based on local approximations of the correlation-exchange potential in the DFT. It is necessary to take explicitly into account dynamical fluctuations to describe these materials. It can be done at best and in a manageable way within the Dynamical Mean Field Theory (DMFT)³. The DMFT captures most of the relevant local quantum dynamical effects of electron correlations. Recent progress in the development of various impurity solvers for the DMFT has opened a way for combining advanced many-body techniques with ab initio methods to build realistic computational schemes for materials with strongly correlated electrons.

The standard way of combining ab initio calculations with the DMFT is via multiorbital Hubbard models. We use the LMTO scheme⁴ to determine the input parameters for multiorbital Hubbard models to be solved within the DMFT. No universal scheme to solve the DMFT equations exactly does exist. Hence, one has to resort to approximate impurity solvers to reach quantitative results from the DMFT. We distinguish essentially two types of DMFT solvers: numerical schemes and analytical methods based on many-body perturbation theory. The former schemes aim at numerically exact quantitative solutions while the latter at analytically controllable schemes. Although analytic methods are not quantita-

tively as accurate as the numerical solutions, they have an appealing feature in that they offer an analytically controllable approach with a direct access to spectral functions on the real frequency axis. Analytic approaches are needed in most situations to complement the numerical solutions so that we can assess the peak structure of spectral functions when performing analytic continuation of numerical results from the imaginary axis of Matsubara frequencies. To gain confidence in approaches based on many-body perturbation theory we should test them in simpler situations and compare their results with available more precise numerical simulations.

In the context of the one band model, extensive comparisons between perturbative approaches such as the IPT and the QMC method have been carried out (see, for example, Refs. 3,5). It is clear that the non-self-consistent IPT is a very accurate approximation. The FLEX method, in its self-consistent and non-self-consistent forms have already been applied to iron and nickel critical discussion, of this method and comparison with QMC has been carried out. It is the aim of this paper to fill this void, and compare diagrammatic schemes with dynamical fluctuations based on two-particle scatterings with finite-temperature Quantum Monte Carlo solution of the DMFT. To this end we use a multiorbital Hubbard model with a simplified kinetic energy so that we can focus our attention on the fundamental features of the transition between weak and strong electron couplings in multiorbital Hubbard models.

A typical form of the Hamiltonian used in dynamical extensions of DFT schemes is

$$H^{\text{Hubb}} = \sum_{\mathbf{R}\lambda, \mathbf{R}'\lambda'} t_{\mathbf{R}\lambda, \mathbf{R}'\lambda'} a_{\mathbf{R}\lambda}^+ a_{\mathbf{R}'\lambda'} + \sum_{\mathbf{R}, \lambda, \lambda' \lambda'' \lambda'''} \langle \mathbf{R}\lambda, \mathbf{R}'\lambda' | V | \mathbf{R}\lambda'' \mathbf{R}\lambda''' \rangle a_{\mathbf{R}\lambda}^+ a_{\mathbf{R}\lambda'}^+ a_{\mathbf{R}\lambda''} a_{\mathbf{R}\lambda'''} \quad (1)$$

where \mathbf{R} are lattice site coordinates and $\lambda = (l\sigma)$ are spin-orbital indices. The hopping term $t_{\mathbf{R}\lambda,\mathbf{R}'\lambda'}$ is determined from a tight-binding LMTO calculation and will be replaced in this comparison study with a model dispersion relation diagonal in the spin-orbital indices. The electron interaction is usually considered only between the d -electrons, since the effect of the lower orbitals is assumed to be described quite well within the TB-LMTO. We assume that the local interaction consists only of direct and exchange terms. We approximate the interaction operator with two parameters only: the Hubbard U and the exchange constant J . In homogeneous cases (without disorder) we can neglect the lattice coordinate and represent the interaction only with a quadruple of spin-orbital indices

$$\langle i\sigma j\sigma' | V | k\sigma l\sigma' \rangle \approx \delta_{ik}\delta_{jl}(1 - \delta_{ij}\delta_{\sigma\sigma'})U + \delta_{il}\delta_{jk}(1 - \delta_{ij})\delta_{\sigma\sigma'}J. \quad (2)$$

This representation can easily be further simplified to a standard matrix in the spin-orbital indices

$$v_{\lambda\lambda'} = (1 - \delta_{\lambda\lambda'})(U - J\delta_{\sigma\sigma'}) . \quad (3)$$

We use this representation of the electron interaction in our many-body treatment of the multiorbital Hubbard model.

II. METHODS

A. Many-body dynamical fluctuations

The effects of the electron interaction on one-particle states are described by the self-energy Σ_λ . Dynamical fluctuations are contained in the two-particle vertex function $\Gamma_{\lambda\lambda'}$. We denote four-momenta $k = (\mathbf{k}, i\omega_n)$ and $q = (\mathbf{q}, i\nu_m)$, and use the Schwinger-Dyson equation to relate the two-particle vertex with the one-particle self-energy. With representation (3) for the electron interaction we can write

$$\Sigma_\lambda(k) = \sum_{\lambda'} \frac{1}{\beta N} \sum_{k'} v_{\lambda\lambda'} G_{\lambda'}(k') \left[1 - \frac{1}{\beta N} \sum_q G_\lambda(k-q) G_{\lambda'}(k'-q) \Gamma_{\lambda\lambda'}(k-q; q, k'-k) \right]. \quad (4)$$

The first term on the r.h.s. of Eq. (4) is the static Hartree term expressing the self-energy in terms of densities. This term in realistic calculations is normally part of the static local density approximation fixing the static particle densities. We hence suppress the Hartree term and use only the vertex contribution to the self-energy as a generator of dynamical fluctuations missing in the DFT.

The simplest approximation on the vertex function $\Gamma_{\lambda\lambda'}$ is the bare interaction $v_{\lambda\lambda'}$. Such an approximation corresponds to second-order perturbation theory (SOPT). The vertex is momentum independent. Even in more advanced approximations we will not use the full momentum dependence of the vertex function. In our treatment we resort only to multiple scatterings of two quasiparticles (FLEX approximations)¹⁰. In this situation the two-particle vertex depends on only a single bosonic four-momentum q . This dependence enters the vertex function via a two-particle bubble. When we deal with multiple electron-hole scatterings the bubble is

$$\Phi_{\lambda\lambda'}(q) = \frac{1}{\beta N} \sum_k G_\lambda(k) G_{\lambda'}(k+q). \quad (5)$$

The self-energy due to dynamical electron-hole (multiple) scatterings can then be represented as

$$\Sigma_\lambda^{eh}(k) = \sum_{\lambda'} \frac{1}{\beta N} \sum_q v_{\lambda\lambda'} G_{\lambda'}(k+q) \Phi_{\lambda\lambda'}(q) \Gamma_{\lambda\lambda'}^{eh}(q). \quad (6)$$

In second-order perturbation theory $\Gamma_{\lambda\lambda'}^{eh} = v_{\lambda\lambda'}$. When we sum ladder electron-hole diagrams we obtain for the vertex function the following representation

$$\Gamma_{\lambda\lambda'}^{eh}(q) = \frac{v_{\lambda\lambda'}}{1 + v_{\lambda\lambda'} \Phi_{\lambda\lambda'}(q)}. \quad (7)$$

Analogously we can construct an approximation with multiple electron-electron scatterings where the self-energy can be represented as

$$\Sigma_\lambda^{ee}(k) = \sum_{\lambda'} \frac{1}{\beta N} \sum_q v_{\lambda\lambda'} G_{\lambda'}(q-k) \Psi_{\lambda\lambda'}(q) \Gamma_{\lambda\lambda'}^{ee}(q). \quad (8)$$

Here we have to use a particle-particle bubble

$$\Psi_{\lambda\lambda'}(q) = \frac{1}{\beta N} \sum_k G_\lambda(k) G_{\lambda'}(q-k). \quad (9)$$

The two-particle vertex $\Gamma_{\lambda\lambda'}^{ee}$ has the same solution as the electron-hole scattering function, Eq. (7), where only we replace the bubble Φ with Ψ .

The third channel of two-particle scatterings is the interaction channel where the electron interaction is screened by electron-hole polarization bubbles. The dynamical self-energy due to this renormalization is then represented as

$$\Sigma_{\lambda}^v(k) = \sum_{\lambda'} \frac{1}{\beta N} \sum_q v_{\lambda\lambda'} G_{\lambda'}(k+q) \Phi_{\lambda\lambda'}(q) \Gamma_{\lambda\lambda'}^v(q) \quad (10)$$

with

$$\Gamma_{\lambda\lambda'}^v(q) = v_{\lambda\lambda'} - \sum_{\lambda''} v_{\lambda\lambda''} \Phi_{\lambda''\lambda'}(q) \Gamma_{\lambda''\lambda'}^v(q). \quad (11)$$

We can treat each channel independently or add all three channels to assess the effect of dynamical fluctuations on the electron self-energy. In the latter case, however,

we have to subtract twice the contribution from second order, since it is identical in all three channels.

The idea of the DMFT is to neglect the momentum dependence of the one-electron propagators in the contributions to the self-energy. We hence use only the local parts of the one-electron propagators, i. e., $G_{\lambda}(\mathbf{k}, i\omega_n) \rightarrow N^{-1} \sum_{\mathbf{k}} G_{\lambda}(\mathbf{k}, i\omega_n) = G_{\lambda}(i\omega_n)$. Then, all the above formulas hold with the replacements $k \rightarrow i\omega_n$, $q \rightarrow i\nu_m$ for fermionic and bosonic momenta, respectively.

The advantage of analytic approaches with multiple two-particle scatterings is the knowledge of the explicit analytic structure of the self-energy. Hence all the above results can be explicitly analytically continued to real frequencies using a straightforward procedure. We explicitly mention only the result for the two-particle electron-hole bubble

$$\Phi_{\lambda\lambda'}(z) = - \int_{-\infty}^{\infty} \frac{d\omega}{\pi} f(\omega - \mu) [G_{\lambda'}(\omega + z) \text{Im} G_{\lambda}(\omega_+) + G_{\lambda}(\omega - z) \text{Im} G_{\lambda'}(\omega_+)] . \quad (12)$$

Up to now we have used the fully renormalized one-electron propagators in the perturbation theory as demanded by conservation laws. However, when we are interested in the one-electron properties of the system, we can relax the demands of thermodynamic consistence and replace the fully renormalized propagator with a partially renormalized one

$$G(z) \longrightarrow \mathcal{G}_0(z) = \frac{G(z)}{1 + \Sigma(z)G(z)}. \quad (13)$$

This propagator goes over into the bare propagator in the atomic limit and does not contain long energy tails due to frequency convolutions in the definition of the self-energy.

This partially non-self-consistent scheme resembles the Iterated Perturbation Theory (IPT). Hence a better description of the transition from weak to strong coupling regimes at the one-particle level, including the metal-insulator transition, is expected from the IPT than from the conserving scheme with fully renormalized propagators.

B. The Quantum Monte Carlo

Among the many methods used to solve the impurity problem we choose the Quantum Monte Carlo method¹¹. There are well known advantages and disadvantages of the QMC method and our choice is spurred by the fact that despite being slower than other methods, the QMC is well controlled, numerically exact method. As an input the QMC procedure gets Weiss function $\mathcal{G}_0(\tau)$ and as an

output it produces Green's function $G(\tau)$. We remind the reader major steps taken in the QMC procedure. Usually one starts with an impurity effective action S :

$$S_{\text{eff}} = - \int_0^{\beta} d\tau d\tau' \sum_{\alpha} c_{\alpha}^{\dagger}(\tau) \mathcal{G}_{0\alpha}^{-1}(\tau, \tau') c_{\alpha}(\tau') + \frac{1}{2} \int_0^{\beta} d\tau \sum_{\alpha, \alpha'} U_{\alpha\alpha'} n_{\alpha}(\tau) n_{\alpha'}(\tau), \quad (14)$$

where $\{c, c^{\dagger}\}$ are fermionic annihilation and creation operators of the lattice problem, $\alpha = \{m, \sigma\}$.

The first what we should do with the action (14) is to discretize it in imaginary time with time step $\Delta\tau$ so that $\beta = L\Delta\tau$, and L is the number of time intervals:

$$S_{\text{eff}} \rightarrow \sum_{\alpha, \tau\tau'} c_{\alpha}^{\dagger}(\tau) \mathcal{G}_{0\alpha}^{-1}(\tau, \tau') c_{\alpha}(\tau') + \frac{1}{2} \sum_{\alpha, \alpha'} U_{\alpha\alpha'} n_{\alpha}(\tau) n_{\alpha'}(\tau). \quad (15)$$

The next step is to get rid of the interaction term U by substituting it by summation over Ising-like auxiliary fields. The decoupling procedure is called the Hubbard-Stratonovich transformation^{12,13}:

$$\exp\{-\Delta\tau\{U_{\alpha\alpha'} n_{\alpha} n_{\alpha'} - \frac{1}{2}(n_{\alpha} + n_{\alpha'})\}\} = \quad (16)$$

$$\frac{1}{2} \sum_{S_{\alpha\alpha'}=\pm 1} \exp\{\lambda_{\alpha\alpha'} S_{\alpha\alpha'} (n_{\alpha} - n_{\alpha'})\},$$

where $\cosh \lambda_{\alpha\alpha'} = \exp(\frac{\Delta\tau U_{\alpha\alpha'}}{2})$ and $S_{\alpha\alpha'}(\tau_l)$ are auxiliary Ising fields at each time slice.

In the one-band Anderson impurity model we have only one auxiliary Ising field $S(\tau_l) = \pm 1$ at *each time slice*, whereas in the multiorbital case number of auxiliary fields is equal to the number of α, α' pairs. Applying the Hubbard-Stratonovich transformation at each time slice we bring the action to a quadratic form with the partition function:

$$Z = \text{Tr}_{\{S_{\alpha\alpha'}(\tau)\}} \prod_{\alpha} \det G_{\alpha, \{S_{\alpha\alpha'}(\tau)\}}^{-1}, \quad (17)$$

where the Green function in terms of auxiliary fields G_{α}^{-1} reads

$$G_{\alpha, \{S_{\alpha\alpha'}\}}^{-1}(\tau, \tau') = \mathcal{G}_{0\alpha}^{-1}(\tau, \tau')e^V - (e^V - 1)\delta_{\tau, \tau'}, \quad (18)$$

with the interaction matrix

$$V_{\tau}^{\alpha} = \sum_{\alpha' (\neq \alpha)} \lambda_{\alpha\alpha'} S_{\alpha\alpha'}(\tau) \sigma_{\alpha\alpha'}, \quad (19)$$

where

$$\begin{aligned} \sigma_{\alpha\alpha'} &= +1 \text{ for } \alpha < \alpha' \\ \sigma_{\alpha\alpha'} &= -1 \text{ for } \alpha > \alpha'. \end{aligned}$$

Once the quadratic form is obtained one can apply Wick's theorem at each time slice and perform the Gaussian integration in Grassmann variables to get the full interacting Green function:

$$G_{\alpha}(\tau, \tau') = \frac{1}{Z} \text{Tr}_{\{S_{\alpha\alpha'}\}} G_{\alpha, \{S_{\alpha\alpha'}\}}^{-1}(\tau, \tau') \prod_{\alpha'} \det G_{\alpha', \{S_{\alpha\alpha'}\}}^{-1}. \quad (20)$$

To evaluate summation in Eq. (20) one uses Monte-Carlo stochastic sampling. The product of determinants is interpreted as the stochastic weight and auxiliary spin configurations are generated by a Markov process with probability proportional to their statistical weight. More rigorous derivation can be found elsewhere^{3, 13}.

Since the QMC method produces results in imaginary time ($G(\tau_m)$ with $\tau_m = m\Delta\tau$, $m = 1 \dots L$) and the DMFT self-consistency equations make use of the frequency dependent Green's functions and self-energies we must have an accurate method to compute Fourier transforms from the time to the frequency domain. This is done by representing the functions in the time domain by a cubic splined functions which should go through original points with condition of continuous second derivatives imposed. Once we know cubic spline coefficients we can compute the Fourier transformation of the splined functions analytically.

III. RESULTS AND DISCUSSION

For purposes of comparison of analytic solutions with numerical ones we employed a simple model with two

degenerate bands, i.e., four spin-orbitals per site and assumed a semi-elliptic density of states (DOS), $\rho_0(E) = \frac{2}{\pi} \sqrt{1 - E^2}$. For simplicity we resorted to the case $J = 0$ and to non-magnetic solutions. We tested second-order perturbation theory together with multiple scatterings from the electron-hole, electron-electron, and interaction channels. Both types of self-consistency are considered, i. e., the full conserving and the partial one with the bath function \mathcal{G}_0 , defined in the IPT Eq. (13). All approximations were analytically continued to real frequencies before being evaluated numerically. A simple iteration procedure with a suitably chosen mixing of the old and new Σ lead to well converged results for moderate values of the pair interaction U . The details of the numerical implementation of multiorbital FLEX-type approximations were described elsewhere^{6, 7, 8, 9, 14}.

First, we compared the analytical approximations among themselves for an intermediate value of the interaction strength, $U = 2$. All energies are given in units of the half-bandwidth of the non-interacting DOS, $D = 1$. When the conserving full self-consistence was used we found that results of SOPT and the electron-electron T -matrix approximation TMA are quite close to each other. The addition of the electron-hole TMA channel worsens the situation. The quasiparticle width gets substantially reduced as shown in Fig. 1 (in the calculation we dropped the third channel, screening by the electron-hole polarization bubbles). The reason why the electron-hole TMA does not improve the situation is quite clear. In the electron-hole TMA, the electron-hole T -matrix becomes divergent at low frequencies when the local interaction U exceeds some critical value U_c . This divergence corresponds to the phase transition from the paramagnetic to the ferromagnetic solution in the lattice case, and it is unphysical for the impurity problem. So, this unphysical divergence overestimates the contribution of the electron-hole T -matrix and the result becomes worse with increasing the interaction strength. As known from the single-band situation, neither of the approximations is able to trace the emergence of satellite Hubbard bands. The high-energy spectrum is shapeless and broadened due to energy convolutions. The situation changes dramatically if we keep only the topological self-consistence of the one-particle propagators obtained from the IPT, see Fig. 2. We can see that second order and the electron-electron TMA show the Hubbard satellite bands in their correct positions. The SOPT scatterings add an additional internal structure to the satellite bands. While the satellite bands gain more weight than it is expected at this interaction strength, the central quasiparticle peak weight is strongly reduced. Too much quasiparticle weight was transferred to the Hubbard bands. In the electron-hole scattering channel we get slight changes in the positions of the Hubbard bands, and slight decrease of the quasiparticle width. Even for rather small interactions $U < 1$ one observes nearly total disappearance of the quasiparticle peak when including the electron-hole channel. This is the main reason why

we excluded the electron-hole TMA scattering channel from further consideration. We compare results of analytical approximations against QMC data in the next figures.

To compare the analytic results with Quantum Monte Carlo simulations, we use only the electron-electron scattering channel in both versions of the self-consistency. Fig. 3 shows the density of states at $U = 1$ calculated within the electron-electron T -matrix approximation along with the one deduced from the QMC. As one can see from the plot, the conserving TMA fits better the quasiparticle peak than the TMA with the IPT bath Green function \mathcal{G}_0 . In addition, the IPT TMA seems to overemphasize the role of the satellite peaks at weak coupling as there are no satellites in the QMC solution for this coupling strength. If we increase the interaction to $U = 2$ (see Fig. 4) and compare the same curves as in the previous plot, we notice that the conserving TMA still very well reproduces the quasiparticle peak, whereas the IPT TMA keeps the tendency to reducing the central peak in favor of the satellites. At this coupling the satellites are formed also in the QMC solution but not as strongly as the IPT TMA predicts. Notice that positions of the satellites reproduced by the IPT solution are rather close to the ones coming from QMC.

As a summary of the FLEX approximation for the symmetric case of the multiband Hubbard model we present dependence of the quasiparticle residue, Z , on the interaction strength, U . It is clear that the closer is the $Z(U)$ dependence for a particular approximation to the QMC curve the better the approximation works in reproducing the quasiparticle properties of the system, including the central peak weight and width. In Fig. 5 we presented the following curves: QMC data are plotted by solid curve with open circle symbols, results of the second order perturbation theory in the cases of fully renormalized one-particle propagators in the self-consistent calculations ($\Sigma = \Sigma[G]$) and partially renormalized by using the iterated perturbation method ($\Sigma = \Sigma[\mathcal{G}_0]$) are given by dashed and dot-dashed lines correspondingly. Concentrating on small and intermediate values of interaction, we can see that in the first case of the full renormalization of the propagators the situation is significantly better as the dashed curve goes much closer to the QMC one than the dot-dashed curve. The electron-electron TMA gives even better results than those obtained from SOPT. Both the electron-electron TMA curves, for the case of the full self-consistency ($\Sigma = \Sigma[G]$) plotted by solid line and the partial one ($\Sigma = \Sigma[\mathcal{G}_0]$), plotted by dotted line with crosses, lay much closer to the QMC data than the SOPT curves. From the two electron-electron TMA curves we make a decision in favor of the one obtained using the fully renormalized one-particle propagators in the self-consistency procedure. This result is quite surprising as it differs from the findings in the case of the one-band Hubbard model, where partially renormalized propagators gave better agreement with Monte Carlo results.

In Fig. 6 we study dependence of DOS calculated by

different methods on orbital degeneracy. We calculated DOS within two- and three-band Hubbard models in the half-filled case using QMC as the tester against two best approximations in FLEX which we found, namely, electron-electron TMA with the full self-consistency ($\Sigma = \Sigma[G]$) and the partial one ($\Sigma = \Sigma[\mathcal{G}_0]$). One can almost immediately notice the main difference between the QMC and FLEX results. The width of quasiparticle (QP) peak in QMC calculation is slightly increased with the degeneracy. This is expectable as while the degeneracy grows the critical U also increases what brings the curve Z versus U dependence (see Fig. 5) to go higher for the larger degeneracy at any particular repulsion. As an example the quasiparticle residue against repulsion at $U = 2$ for degeneracy $N = 6$ will be above the curve in Fig. 5 corresponding to degeneracy $N = 4$. FLEX results show opposite dependence: the QP width decreases with increasing degeneracy. We should also notice that this wrong tendency is stronger for the partial (IPT) self-consistency. The reason for such kind of behavior can lay in a limited set of diagrams treated in FLEX what results in an insufficient screening for higher degeneracy.

While a good agreement with the self-consistent FLEX scheme is found for two and three bands, it is important to stress that this cannot persist for very large degeneracy. It has been shown¹⁵ that in the exact solution of the DMFT equations for large N the critical U where the Mott transition takes place at zero temperature, scales linearly with N . This implies that *for fixed* U the quasiparticle residue, which has an approximate expression, $Z = 1 - U/U_{c2}$ increases and eventually approaches unity with increasing orbital degeneracy. This remarkable screening effect in the multiorbital degenerate Hubbard model is not captured by the FLEX approach which displays the opposite trend, as described in Fig. 7.

When we move off the electron-hole symmetric case, the situation changes quite a bit. The quasiparticle peak is no longer so strongly suppressed in the FLEX approximations and even the conserving TMA starts to develop a satellite peak. Fig. 8 demonstrates this trend for $n = 0.8$. We notice almost no difference in the form of the central peak in the two different self-consistent versions of the multiple electron-electron scatterings. The IPT version retains its tendency to overemphasize the width of the satellite peaks and produces an incorrect position of the upper Hubbard band. The conserving TMA shows a shoulder behavior where the QMC displays the hole satellite. The less pronounced electron peak cannot be traced neither in the IPT TMA nor in the conserving TMA.

IV. CONCLUSION

In summary, we compared multiband implementation of the FLEX procedure within the framework of the two-band model with semi-elliptic non-interacting DOS against the Quantum Monte Carlo method. Obtained

results indicate the best agreement with the QMC data in region of moderate Coulomb interaction, ($U \leq 2$), for the FLEX without the electron-hole TMA and with fully renormalized one-particle propagators in the self-consistent calculations ($\Sigma = \Sigma[G]$). Our finding is somewhat different from that for the one-band Hubbard model, where the best match was found for the one-particle propagators partially renormalized by using the iterated perturbation method ($\Sigma = \Sigma[\mathcal{G}_0]$). In the multi-band situation for intermediate band degeneracy and small to intermediate U the self-consistent version describes the quasiparticle features in good agreement with QMC. On the other hand, there is no hint in the self-consistent calculation of an incipient Mott transition, as in the one band case¹⁶, while the non-self-consistent scheme clearly gives a hint that a Mott transition will take place, albeit at a very small unphysical value of U , due to an improper screening of this interaction.

Unsufficient screening due to a limited set of diagrams treated in FLEX results in a quasiparticle weight underestimation with increasing degeneracy in the system. For non-symmetric case, FLEX approximation has tendency to overestimate the QP width and underestimate the Hubbard bands weight given their correct position in

the case of conserving TMA.

Acknowledgments

The research was carried out by V.D., V.J., and J.K. within the project AVOZ1-010-914 of the Academy of Sciences of the Czech Republic and supported in part by a grant ME-383 of the Ministry of Education, Youth, and Sports of the Czech Republic. We (V.O., X.D., K.H., and G.K.) acknowledge support from a grant nsf-int9907893 U.S.-Czech Materials Research on Many-Body Correlations in Calculations of Realistic Electronic Structure of Solids. We would like to thank A. Lichtenstein for extensive and fruitful discussions of the works of FLEX. We also would like acknowledge a warm hospitality extended to four of us (V.J, V.O., X.D. and G.K.) during our stay at Kavli Institute for Theoretical Physics during the workshop “Realistic Theories of Correlated Electron Materials” where part of this work has been carried out. The work was supported by the NSF grant DMR-00096462.

* Electronic address: drchal@fzu.cz

- ¹ P. Hohenberg and W. Kohn, Phys. Rev. **136**, B864 (1964).
- ² W. Kohn, Rev. Mod. Phys. **71**, 1253 (1999).
- ³ A. Georges, G. Kotliar, W. Krauth, and M. Rozenberg, Rev. Mod. Phys. **68**, 13 (1996).
- ⁴ I. Turek, V. Drchal, J. Kudrnovský, M. Šob, and P. Weinberger, *Electronic Structure of Disordered Alloys, Surfaces and Interfaces* (Kluwer, Boston-London-Dordrecht, 1997).
- ⁵ H. Kajueter and G. Kotliar, Phys. Rev. Lett. **77**, 131-134 (1996).
- ⁶ V. Drchal, V. Janiš, and J. Kudrnovský, in *Electron Correlations and Materials Properties* edited by A. Gonis et al., (Kluwer Academic/Plenum Publishers, NY, 1999), p. 273.
- ⁷ V. Drchal, V. Janiš, and J. Kudrnovský, Phys. Rev. B **60**, 15664 (1999).
- ⁸ M. I. Katsnelson and A. I. Lichtenstein, J. Phys.: Cond. Matt. **11**, 1037 (1999).
- ⁹ M. I. Katsnelson and A. I. Lichtenstein, Phys. Rev. B **61**, 8906 (2000).
- ¹⁰ N. E. Bickers and D. J. Scalapino, Ann. Phys. (N.Y.) **193**, 206 (1989).
- ¹¹ J. E. Hirsch and R. M. Fye, Phys. Rev. Lett. **56**, 2521 (1986).
- ¹² J. E. Hirsch, Phys. Rev. B **28**, 4059 (1983).
- ¹³ K. Takegahara, J. Phys. Soc. Jpn. **62**, 1736 (1992).
- ¹⁴ V. Drchal, V. Janiš, and J. Kudrnovský, in *Electron Correlations and Materials Properties 2* edited by A. Gonis et al., (Kluwer Academic/Plenum Publishers, NY, 2003), p. 341.
- ¹⁵ S. Florens, A. Georges, G. Kotliar, O. Parcollet, Phys. Rev. B **66**, 205102 (2002).
- ¹⁶ B. Menge and E. Müller-Hartmann, Z. Phys. B **82**, 237

(1991).

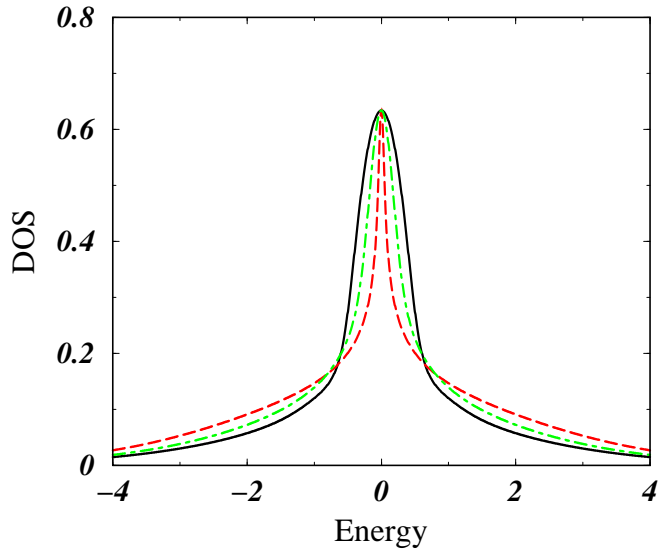


FIG. 1: Densities of states for $U = 2$, $n = 2$ (half-filled case) calculated within the second-order perturbation theory (dot-dashed line), electron-electron TMA (solid line), and electron-hole TMA (dashed line). The one-particle propagators are fully renormalized in the self-consistent calculations ($\Sigma = \Sigma[G]$).

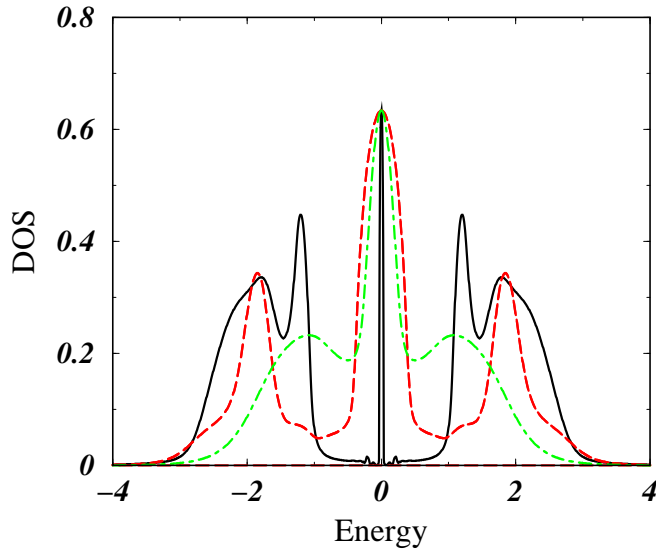


FIG. 2: Densities of states for $U = 2$, $n = 2$ (half-filled case) calculated within the second-order perturbation theory (solid line), electron-electron TMA (dashed line), and electron-hole TMA (dot-dashed line). The one-particle propagators are partially renormalized by using the iterated perturbation method ($\Sigma = \Sigma[\mathcal{G}_0]$).

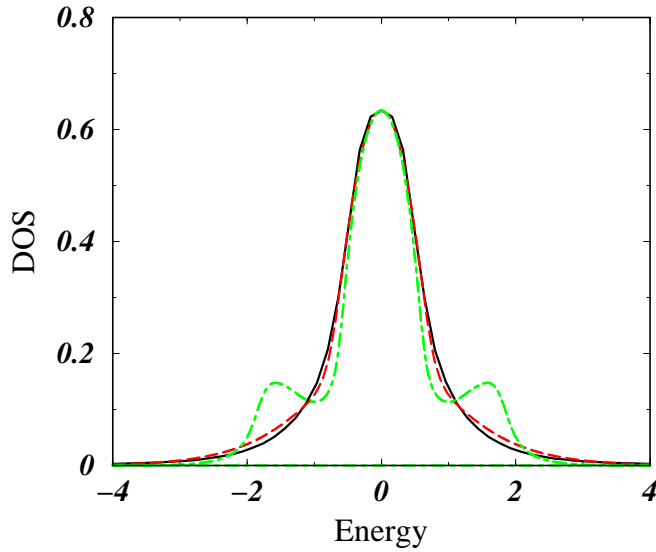


FIG. 3: Densities of states for $U = 1.0$, $n = 2$ (half-filled case) calculated within the electron-electron TMA using the full renormalization of the one-particle propagators (dashed line) and partial renormalization using the IPT (dot-dashed line) compared with the result of quantum Monte Carlo method (solid line).

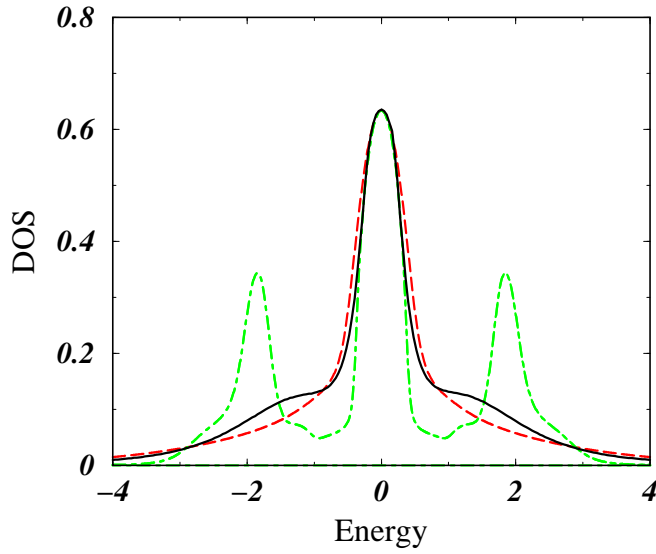


FIG. 4: Densities of states for $U = 2.0$, $n = 2$ (half-filled case) calculated within the electron-electron TMA using the full renormalization of the one-particle propagators (dashed line) and partial renormalization using the IPT (dot-dashed line) compared with the result of quantum Monte Carlo method (solid line).

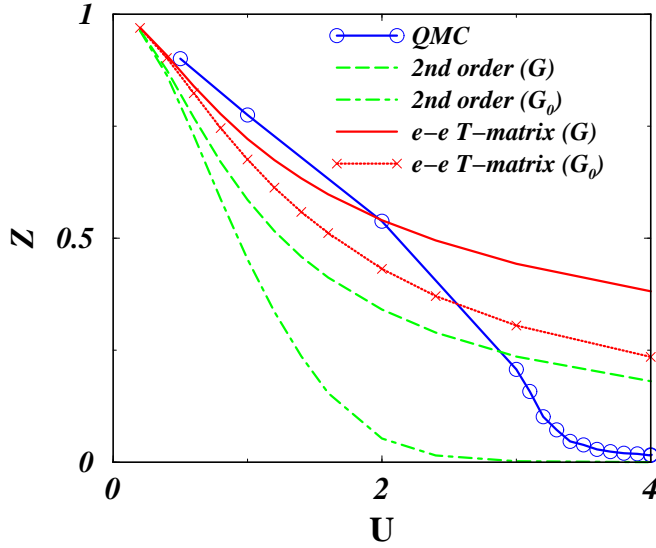


FIG. 5: Dependence of the quasiparticle residue Z on Coulomb repulsion U calculated within the electron-electron TMA (solid and dotted with crosses lines) and the second-order perturbation theory (dashed and dot-dashed lines) using the full renormalization of the one-particle propagators and partial renormalization using the IPT correspondingly. QMC results are plotted by solid line with circle symbols.

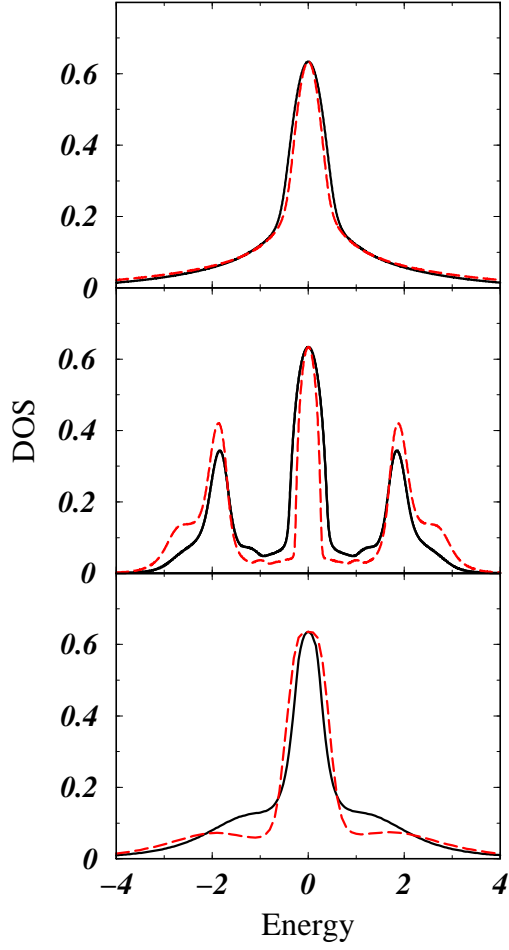


FIG. 6: Densities of states for $U = 2.0$, $n = 2$ in the two-band model (solid lines) and $n = 3$ in the three-band model (dashed lines) (both cases correspond to half-filled case) calculated within the electron-electron TMA using the full renormalization of the one-particle propagators (upper panel) and partial renormalization using the IPT (middle panel) compared with the result of quantum Monte Carlo method (lower panel).

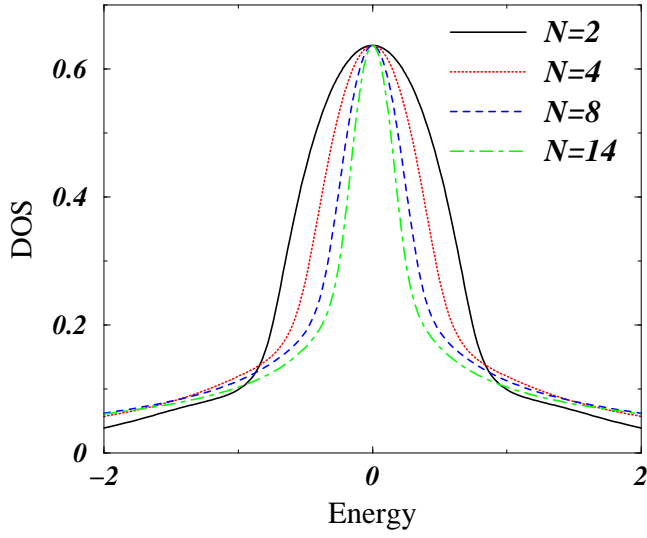


FIG. 7: Densities of states for $U = 2.0$ (n is kept at the half-filling) calculated within the electron-electron TMA using the full renormalization of the one-particle propagators for different degeneracy (see the legend).

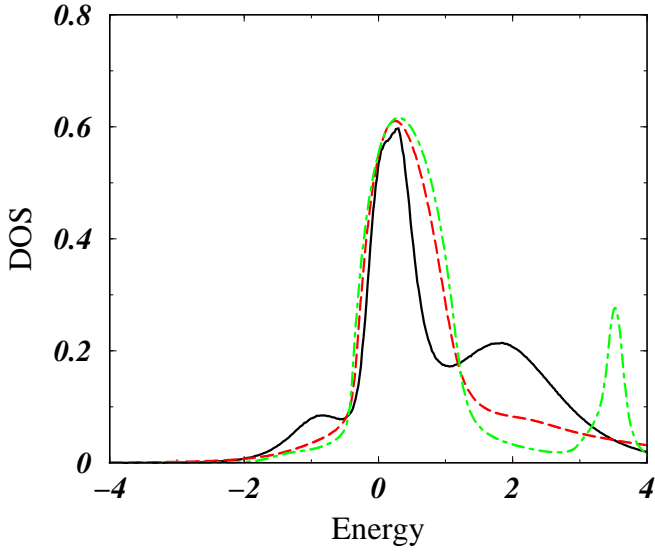


FIG. 8: Densities of states for $U = 2.0$, $n = 0.8$ (partially filled band) calculated within the electron-electron TMA using the full renormalization of the one-particle propagators (dashed line) and partial renormalization using the IPT (dot-dashed line) compared with the result of quantum Monte Carlo method (solid line).